

# Orbital Alignment and Morphology of Pentacene Deposited on Au(111) and SnS<sub>2</sub> Studied Using Photoemission Spectroscopy

P. G. Schroeder, C. B. France, J. B. Park, and B. A. Parkinson\*

*Department of Chemistry, Colorado State University, Fort Collins, Colorado 80523*

*Received: March 21, 2002; In Final Form: September 30, 2002*

The energy level alignment at the pentacene/Au(111) and pentacene/SnS<sub>2</sub> interfaces was determined using in situ thin film deposition in combination with X-ray and ultraviolet photoemission spectroscopy (UPS). The organic thin films were grown by vapor deposition in multiple steps and then sequentially characterized in situ after each growth step. The pentacene/Au(111) interface is an ohmic contact that yielded a strong (0.95 eV) interfacial dipole barrier. The vacuum-cleaved SnS<sub>2</sub> single crystal substrates provided clean, atomically flat and chemically inert surfaces, allowing for the investigation of the core level energy shifts and interface dipoles without interference from chemical reactions or effects of the substrate morphology. Low-intensity X-ray photoemission work function measurements enabled the detection of the overlayer thickness-dependent onset of charging in the UPS measurements. This allowed for precise determination of the position of the highest occupied molecular orbital of the organic molecules at the investigated interfaces. Differences in the orientation of the pentacene molecules on the two substrates were proposed based on analysis of the UPS spectra, scanning tunneling microscopy results of their films, and atomic force microscopy images of thick pentacene layers.

## I. Introduction

Pentacene has recently been determined to be one of the most promising candidates for organic thin film field effect transistors (FET)<sup>1–3</sup> or organic-based photovoltaic devices<sup>4,5</sup> due to its high field effect mobility of 1.4 cm<sup>2</sup>/V·s for the single crystal<sup>6</sup> at room temperature and upward of 10<sup>4</sup>–10<sup>5</sup> cm<sup>2</sup>/V·s at very low temperature.<sup>7</sup> Both single crystals and thin films of pentacene have been used for fabrication of transistor devices. Typically, a Si/SiO<sub>2</sub> substrate has been used as the gate electrode, while gold has been used as the contact material for the source and drain electrodes. There have been several studies of pentacene deposited on Si or SiO<sub>2</sub>,<sup>8–10</sup> however, there have been very few studies into the electronic and morphological properties of the pentacene/gold interface. Device performance can be understood and perhaps improved if a detailed picture of the orbital alignment of the organic molecule with the Fermi level of the metal can be achieved. The picture will then predict the existence of electron or hole transfer barriers that influence the current–voltage behavior of devices. Determination of the barrier offsets between an organic semiconductor film and a contact/electrode material to elucidate the electronic characteristics of the interface can be used to greatly enhance device performance. Determining the energy level offsets at the pentacene/SnS<sub>2</sub> interface probes the properties of a p–n type heterojunction involving an organic and inorganic semiconductor. The nearly atomically flat van der Waals surface of the SnS<sub>2</sub> substrate also functions as a model substrate to further investigate the fundamental properties of the organic/semiconductor interface.

A common procedure for determining the energy level offsets at interfaces is photoemission spectroscopy.<sup>11–17</sup> Ultraviolet photoelectron spectroscopy (UPS) is used to determine the work function and position of the occupied molecular orbital or valence band states of the sample. X-ray photoelectron spec-

troscopy (XPS) is also included in our measurements to distinguish the interface dipole from either the band bending or the final state screening related shifts in the work function, as well as to assist in the determination of the growth modes of the organic films.

## II. Experimental Section

All in situ experiments were performed in a commercial Omicron Multi-Probe ultrahigh vacuum (UHV) apparatus (base pressure =  $5 \times 10^{-11}$  mbar) equipped with variable temperature scanning tunneling microscopy (VT STM), low-energy electron diffraction (LEED), temperature-programmed desorption (TPD), XPS, UPS, and a VSW EA125 single channel hemispherical analyzer. The organic physical vapor deposition chamber (base pressure =  $1 \times 10^{-9}$  mbar) was attached to the analysis chamber allowing the samples to be prepared in situ. The 1 cm<sup>2</sup> SnS<sub>2</sub> crystal [Cl<sup>−</sup> doped ( $8 \times 10^{16}$  cm<sup>−3</sup>)] was cleaved in situ using a glued on metal foil and characterized with XPS and UPS prior to deposition. The gold film was prepared by heating a mounted 2 cm<sup>2</sup> mica sample for 24 h in UHV to 300 °C to evaporate surface contaminants. Gold was then evaporated from a tungsten wire basket onto the heated mica substrate. Annealing to 350 °C for 5 h yielded the Au(111) surface that showed the ( $23 \times \sqrt{3}$ ) reconstruction as determined with LEED and STM. Small molybdenum clips were attached to the outer edges of the sample to ensure that the gold film would be electrically grounded. The pentacene films were grown by sublimation from a resistively heated boron nitride crucible (source temperature was 142 °C). The source was held at 120 °C for 12 h prior to deposition to outgas lower vapor pressure contaminants. The pentacene was deposited at a rate of 4 Å/min, monitored using a Leybold quartz crystal microbalance (QCM). After each growth step, the samples were characterized in situ using XPS

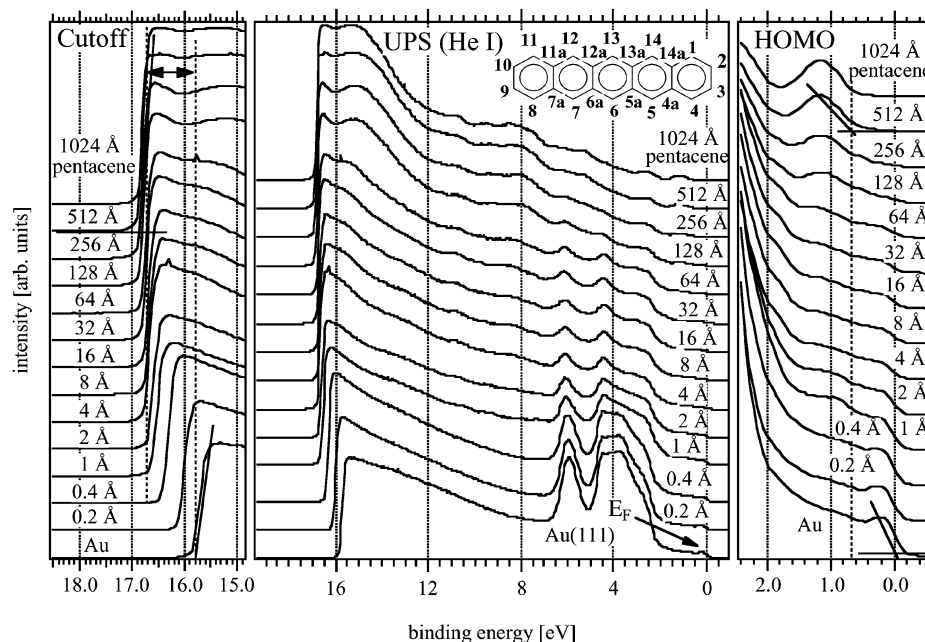


**Figure 1.** UPS He I spectra of pentacene deposited on Au(111). The center portion shows the full spectra on a binding energy scale. The spectra on the left are the magnified HBEC used to determine the sample work function. The right side shows the magnified region where the gold Fermi edge and the HOMO peak of the pentacene are observed. The molecular structure of pentacene is shown with the IUPAC numbering system for the C atom positions.

(Mg K $\alpha$ , 50 eV pass energy) and UPS (HeI, 21.21 eV; and HeII, 40.81 eV, both with 10 eV pass energy) in normal emission. A  $-5.00$  V bias was applied to the sample for the UPS measurements to separate the sample and spectrometer high binding energy cutoffs (HBECs). The SnS<sub>2</sub> substrates were mounted on a pedestal elevated 5 mm above the sample plate to prevent stray electrons from the manipulator assembly interfering with the UP spectra. Elevation of the gold sample was not necessary due to the sufficiently large sample size. The spectrometer was calibrated to yield the standard values<sup>17–19</sup> of 75.13 eV for the Cu 3p and 932.66 eV for the Cu 2p<sub>3/2</sub> emission lines on an Ar<sup>+</sup>-sputtered Cu sample. The binding energy zero was determined using the Fermi level position of the Cu sample. The overall analyzer resolution of 0.20 eV was determined from the width of the Cu Fermi edge. Therefore, work function and the highest occupied molecular orbital (HOMO) cutoff positions, determined from the HBECs and HOMO onsets of UP spectra, were corrected for the analyzer broadening by adding/subtracting 0.1 eV. XPS core level peak positions were determined by a fitting routine using IGOR Pro (Wavemetrics) data evaluation software. A vacuum-deposited pentacene film on quartz was used to obtain the solid state absorption spectrum that was measured using a Varian Cary-500 UV–vis–NIR spectrophotometer.

Atomic force microscopy (AFM) was performed in tapping mode using a Digital Instruments nanoscope III multiprobe AFM. The cantilevers used were Nanodevices Metrology Probes Multi75 with a force constant of 3 N/m and a resonance frequency of approximately 75 kHz.

### III. Results

**A. Pentacene on Au(111).** The pentacene film was grown in multiple steps on a vacuum-deposited gold substrate. The UPS (He I) for pentacene on gold is shown in Figure 1. The full spectra are shown in the center part of the figure with the bottom spectra being the UPS for the bare gold substrate. The changes in the band structure are evident as thicker layers of

pentacene are deposited on the substrate. The HBEC is shown expanded and normalized in the left part of Figure 1. A very significant shift in the HBEC between the bare gold substrate and the one monolayer of pentacene (about 4 Å) is clearly evident. This indicates the existence of a strong charge dipole at this interface. The shift in the HBEC is more gradual after this point, indicating only minimal band bending into the bulk of the pentacene. On the right part of Figure 1, the Fermi edge of the gold (0 eV) is shown along with the evolution of the HOMO peak of the pentacene as the film thickness is gradually built up to over 1000 Å.

The pentacene on gold interface is a Schottky barrier; therefore, the offsets of interest are the barrier height between the Fermi level of the Au(111) and the HOMO<sub>cutoff</sub> of the pentacene (hole injection barrier ( $\Phi_{bh}$ )), and the lowest unoccupied molecular orbital (LUMO)<sub>cutoff</sub> (electron injection barrier ( $\Phi_{be}$ )) of the pentacene. The work function of the gold substrate was determined by subtracting the HBEC of the UP spectra from the source energy (21.21 eV) yielding  $\Phi = 5.47$  eV, which is slightly higher than recorded literature values.<sup>20</sup> The HOMO<sub>cutoff</sub> of the 512 Å layer of pentacene was determined to be 0.65 eV from the lowest binding energy edge of the spectra. The work function for the pentacene film at this same thickness was measured to be 4.42 eV. This gives a total work function shift ( $\Delta\Phi$ ) of

$$\Delta\Phi = \Phi(\text{Au}) - \Phi(512 \text{ Å pentacene}) = 5.47 \text{ eV} - 4.42 \text{ eV} = 1.05 \text{ eV}$$

To more precisely determine the energy level offsets of an electronic interface, any band bending that might be occurring in the organic material or polarization energy-related shifts that occur at the interface need to be included in the evaluation. Such shifts are determined by measurement of the shift of the core level photoemission peaks using XPS. The core level spectra are shown in Figure 2, where C 1s photoemission peaks for the pentacene film are on the left and the Au 4f photoemis-

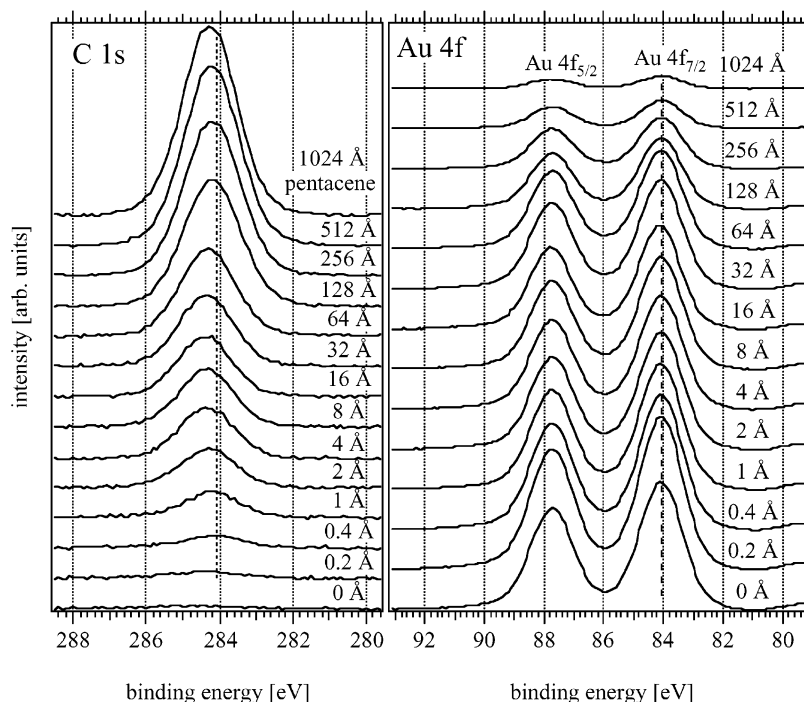


**Figure 2.** XPS of the pentacene C 1s (left) and substrate Au 4f (right) peaks as a function of pentacene layer thickness.

sion peaks are the on the right. The Au 4f peaks will not be subject to any band bending-related shifts. There is a subtle (0.10 eV) shift in the C 1s spectra between the 0.4 Å layer, the lowest coverage where a Gaussian–Lorentzian function could be fit to the spectra, and the 512 Å layer of pentacene.

Regardless of the origin of the core level shift, neither band bending nor changes in the polarization environment should contribute to the magnitude of any charge dipole occurring at the interface. So the core level shift should still be subtracted out from the total work function shift to precisely determine the magnitude of the interface dipole barrier. Subtracting the C 1s core level shift ( $\Delta C\ 1s$ ) from the total shift in the work function of the sample ( $\Delta\Phi$ ) yields the magnitude of the interface dipole barrier (eD):

$$eD = \Delta\Phi - \Delta C\ 1s = 1.05\text{ eV} - 0.10\text{ eV} = 0.95\text{ eV}$$

The magnitudes of the core level shift and interface dipole are displayed graphically in Figure 3, where the total work function shift (filled symbols) and the C 1s core level shift (open symbols) are plotted vs pentacene film thickness. The curves are aligned at the 512 Å point, which is the thickest point where sample charging effects do not influence the measurements.<sup>12,15</sup>

The hole and electron injection barriers ( $\Phi_{bh}$  and  $\Phi_{be}$ ) at the pentacene/gold interface are determined by comparing the positions of the HOMO/LUMO of the pentacene relative to the Fermi level of the gold. Subtracting the core level shift in the pentacene ( $\Delta C\ 1s$ ) from the HOMO<sub>cutoff</sub> at the 512 Å layer results in the hole injection barrier:

$$\Phi_{bh} = \text{HOMO}_{\text{cutoff}}(512\text{ Å pentacene}) - \Delta C\ 1s = 0.65\text{ eV} - 0.10\text{ eV} = 0.55\text{ eV}$$

The position of the LUMO cannot be measured directly using UPS; however, it can be estimated by incorporating the optical absorption gap of the pentacene thin film into the evaluation. The visible absorption spectrum of a pentacene thin film deposited on a quartz substrate is shown in Figure 4. The

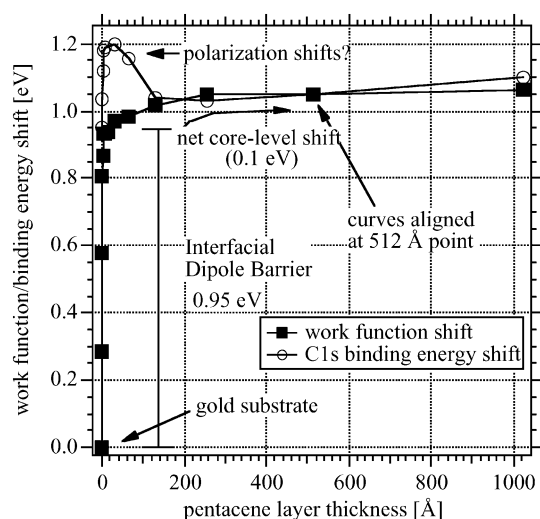


**Figure 3.** Pentacene on Au(111): plot of the C 1s binding energy shift and work function shift as a function of the pentacene layer thickness. The difference between these shifts yields the magnitude of the interfacial dipole barrier.

maximum absorption peak occurs at 668 nm corresponding to a band gap ( $E_g$ ) of 1.85 eV. It is important to note that the optical gap value for organic materials can be used only as an estimate for electronic HOMO–LUMO gap since the large excitonic binding energy of the molecules of the order of 0.5 eV is not accounted for.<sup>21</sup> Subtracting the band gap ( $E_g$ ) from the hole injection barrier results in the electron injection barrier height:

$$\Phi_{be} = \Phi_{bh} - E_g(\text{pentacene}) = 0.55\text{ eV} - 1.85\text{ eV} = -1.30\text{ eV}$$

The negative sign of this barrier height indicates that the  $\Phi_{be}$  points upward into the pentacene layer from the Fermi level of the gold in the opposite direction of the  $\Phi_{bh}$ .

The ionization potential ( $E_{ion}$ ) of the pentacene was determined by adding the work function of the pentacene, at the 512

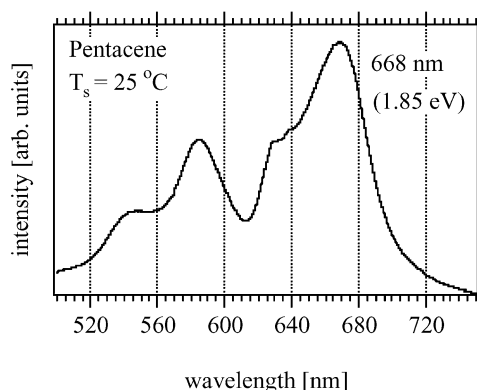


**Figure 4.** Optical absorption spectra of a pentacene film used to estimate the band gap.

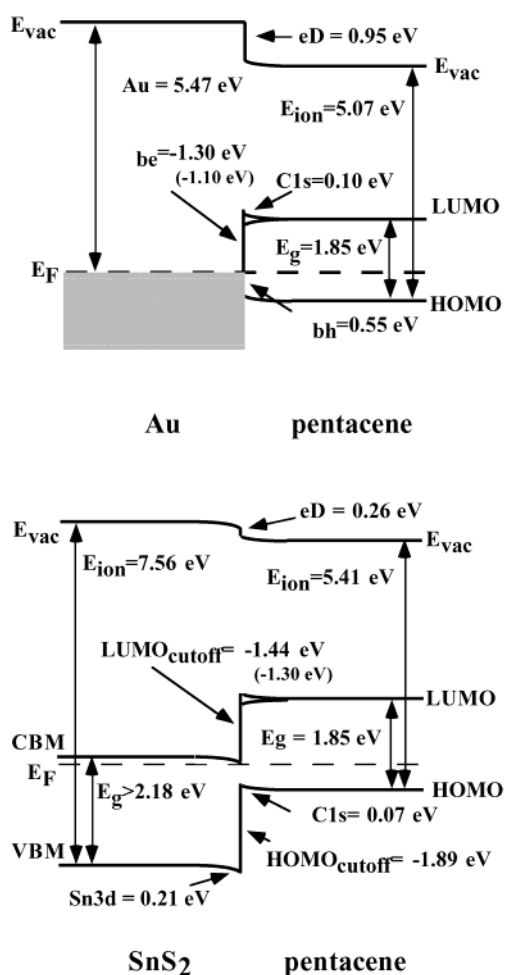


**Figure 5.** Band diagrams of the pentacene/Au(111) (top) and pentacene/SnS<sub>2</sub> (bottom) interfaces.

Å thickness, to the HOMO<sub>cutoff</sub> of the same spectra yielding

$$E_{\text{ion}} = \Phi(512 \text{ Å pentacene}) + \text{HOMO}_{\text{cutoff}}(512 \text{ Å pentacene}) = 4.42 \text{ eV} + 0.65 \text{ eV} = 5.07 \text{ eV}$$

This ionization potential is consistent with the measured value of 4.85 eV for an amorphous pentacene film.<sup>22</sup> The energy level alignment of the pentacene/Au interface resulting from all of the measurements is shown in the band diagram in the top of Figure 5.

**B. Pentacene on SnS<sub>2</sub>.** The same procedure was applied to the pentacene/SnS<sub>2</sub> interface to investigate the behavior of

pentacene at the interface of an inorganic semiconductor. Figure 6 shows the UP spectra sequence for the pentacene/SnS<sub>2</sub> interface. The bottom spectrum was measured on the vacuum-cleaved SnS<sub>2</sub> crystal. The upper spectra were measured after each of the pentacene deposition steps, starting with a nominal coverage of 0.1 Å and progressively increasing the thickness up to the final coverage of 1024 Å. The center part of Figure 6 shows the complete spectra revealing the evolution of the valence band photoemission peaks between the SnS<sub>2</sub> substrate and the bulk pentacene film. The left part of this figure shows a magnification of the normalized HBEC region of the UP spectra. A magnified spectral region of the valence band edge/HOMO of the sample is shown on the right side of Figure 6.

The core level shifts were again measured with XPS. The Sn 3d emission peaks are shown in the left part of Figure 7. The shift in the Sn 3d emission line from the SnS<sub>2</sub> substrate, caused by the pentacene deposition, was determined to be  $\Delta\text{Sn } 3d = 0.21 \text{ eV}$  shift between the vacuum-cleaved substrate (binding energy = 486.93 eV) and the thick pentacene film (binding energy = 487.14 eV).

The C 1s spectra are shown on the right side of Figure 7 where the increasing intensity of the C 1s peak is evident. A trace quantity (estimated to be about 1–3% surface coverage) of a carbon contamination peak, at a significantly higher (>1 eV) binding energy than the peak attributed to the pentacene, was detected on the vacuum-cleaved SnS<sub>2</sub> substrate. A peak-fitting procedure that incorporates both the contaminate C 1s peak and the C 1s peak for the organic layer was used to deconvolute the contaminate peak from the pentacene-related peaks that start to dominate the spectrum at about 2–4 Å coverages. Details of this fitting procedure, described in previous work,<sup>23</sup> allowed for the separation of the contamination and the pentacene C 1s peaks to determine the actual binding energy of the C 1s peak that is attributed to the deposited pentacene. An example of this procedure, in the bottom right part of Figure 7, shows the peak for the 2 Å thick pentacene film fit with a Gaussian–Lorentzian function. The initial binding energy of the pentacene C 1s peak was determined to be 284.15 eV, that is, the average C 1s binding energy for the 0.2, 0.4, 1, and 2 Å growth steps. The binding energy for the thick pentacene film (512 Å) was determined to be 284.22 eV. This gives a small core level shift ( $\Delta\text{C } 1s$ ) of 0.07 eV in the pentacene film.

Adding the core level shifts of the Sn 3d peaks and the pentacene C 1s emission peaks yields the total core level shift [CL(tot)] magnitude across the interface

$$\text{CL}(\text{tot}) = \Delta\text{C } 1s + \Delta\text{Sn } 3d = 0.07 \text{ eV} + 0.21 \text{ eV} = 0.28 \text{ eV}$$

The total shift of the work function  $\Delta\Phi$  between the vacuum-cleaved substrate of the SnS<sub>2</sub> [ $\Phi(\text{SnS}_2)$ ] and the 512 Å layer of the pentacene [ $\Phi(512 \text{ Å pentacene})$ ] was determined to be

$$\Delta\Phi = \Phi(\text{SnS}_2) - \Phi(512 \text{ Å pentacene}) = 5.30 \text{ eV} - 4.76 \text{ eV} = 0.54 \text{ eV}$$

Subtracting the total core level shift [CL(tot) = 0.28 eV] from the work function shift gives the magnitude of the interface dipole

$$eD = \Delta\Phi - \text{CL}(\text{tot}) = 0.54 \text{ eV} - 0.28 \text{ eV} = 0.26 \text{ eV}$$

The energy offset ( $\Delta\text{HOMO}_{\text{cutoff}}$ ) between the VBM of the SnS<sub>2</sub> substrate and the HOMO of the pentacene film was



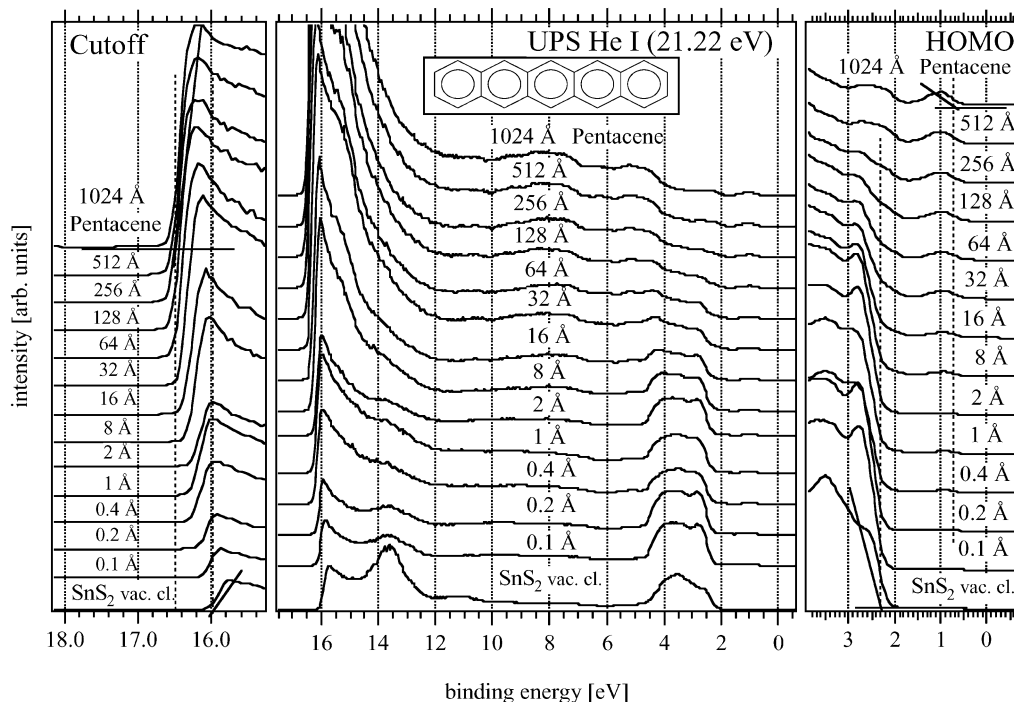


**Figure 6.** UPS He I of pentacene deposited on SnS<sub>2</sub>. The center portion consists of the full spectra. The left is the HBEC, while the right is the magnified region of the valence band maxima/HOMO of the SnS<sub>2</sub> and pentacene.

evaluated by subtracting the initial VBM position of the SnS<sub>2</sub> (2.26 eV) and the total core level shifts [CL(tot) = 0.28 eV] from the HOMO<sub>cutoff</sub> of the 512 Å layer of pentacene yielding

$$\begin{aligned}\Delta\text{HOMO}_{\text{cutoff}} &= \text{HOMO}_{\text{cutoff}}(512 \text{ Å pentacene}) - \\ &\quad \text{VBM}(\text{SnS}_2) - \text{CL}(\text{tot}) = 0.65 \text{ eV} - \\ &\quad 2.26 - 0.28 \text{ eV} = -1.89 \text{ eV}\end{aligned}$$

The conduction band minimum (CBM)/LUMO offset was determined by including the optical band gaps of the SnS<sub>2</sub> and pentacene into the evaluation. A common value of the band gap used for the SnS<sub>2</sub> crystal is 2.18 eV, which is the average of the optical absorption measurements given in the literature.<sup>24</sup> The electronic band gap, however, is most likely several tenths of an electronvolt larger and needs to be at least as large as the distance between the VBM and the Fermi level (>2.26 eV), so a value of 2.30 eV provides a reasonable estimate. The optical band gap for the pentacene was 1.85 eV as previously used. The offset between the LUMO of the pentacene and the CBM of the SnS<sub>2</sub> was determined by subtracting the difference of the band gaps from  $\Delta\text{HOMO}_{\text{cutoff}}$  (−1.30 eV) and yielded

$$\begin{aligned}\Delta\text{LUMO}_{\text{cutoff}} &= \Delta\text{HOMO}_{\text{cutoff}} - (E_g(\text{pentacene}) - \\ &\quad E_g(\text{SnS}_2)) = -1.89 - (1.85 - 2.30 \text{ eV}) = -1.44 \text{ eV}\end{aligned}$$

The negative values of both the  $\Delta\text{HOMO}_{\text{cutoff}}$  and the  $\Delta\text{LUMO}_{\text{cutoff}}$  indicate that the HOMO and LUMO of the pentacene are at a lower binding energy than the VBM and CBM, respectively, of the SnS<sub>2</sub> crystal. A schematic diagram of the complete electronic structure of the interface is shown in the bottom part of Figure 5. The ionization potential of the SnS<sub>2</sub> was evaluated by adding the VBM position (2.26 eV) to the work function (5.30 eV), yielding

$$\begin{aligned}E_{\text{ion}}(\text{SnS}_2) &= \text{VBM}(\text{SnS}_2) + \Phi(\text{SnS}_2) = 2.26 + \\ &\quad 5.30 \text{ eV} = 7.56 \text{ eV}\end{aligned}$$

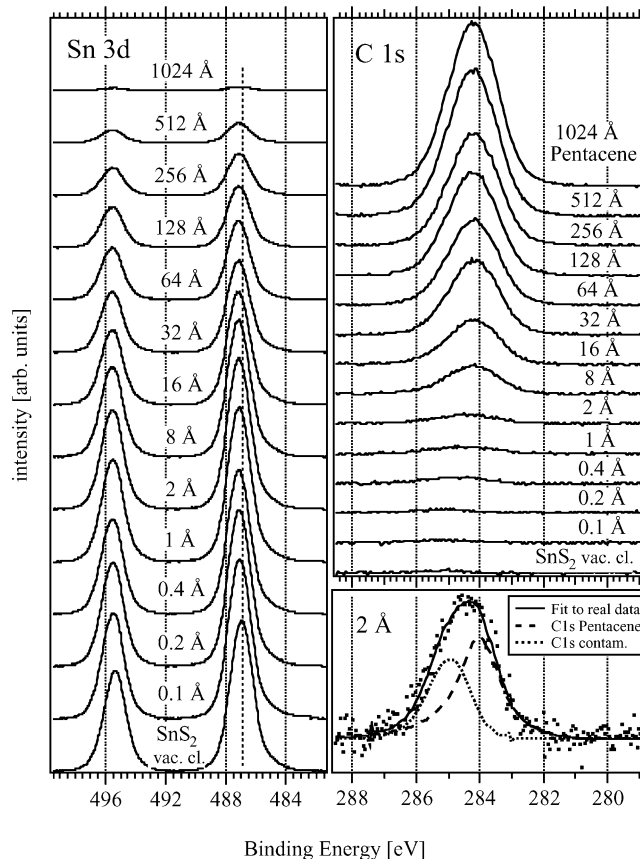


**Figure 7.** XPS core-level peaks of Sn 3d (left) and C 1s (right) for the pentacene on the SnS<sub>2</sub> interface. The inset at the lower right shows the curve fitting to separate the C 1s signal of the pentacene from that of trace contamination.

The ionization potential for the pentacene grown on SnS<sub>2</sub> was similarly determined by adding the position of the HOMO<sub>cutoff</sub>(512 Å pentacene) to the work function of the same

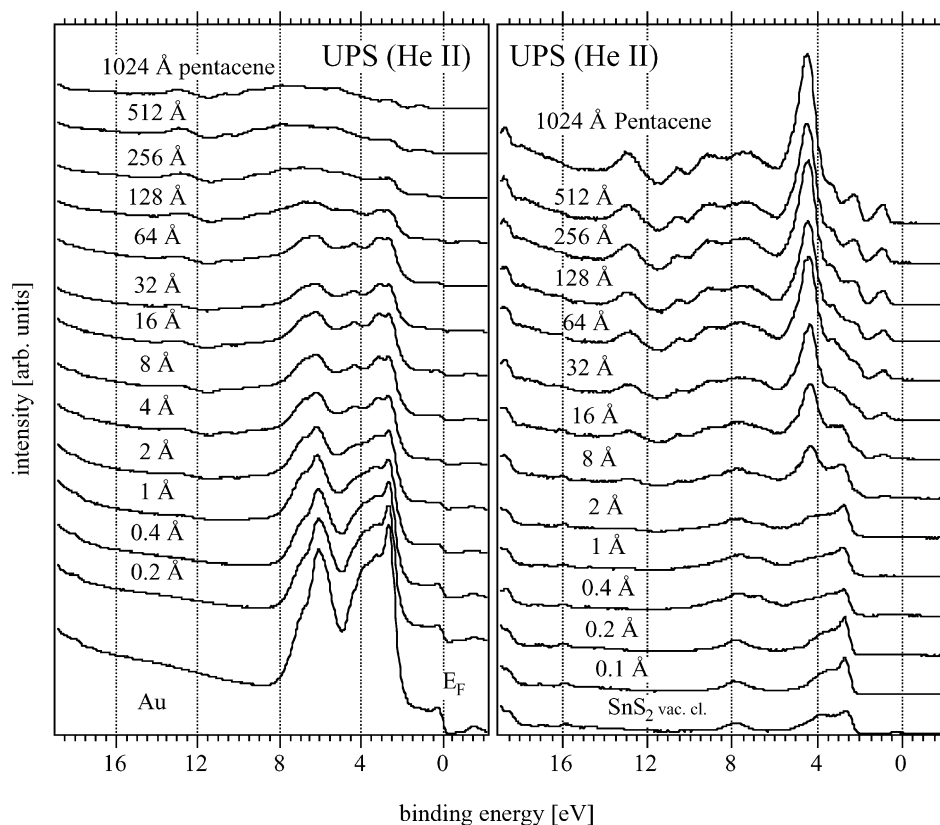


**Figure 8.** Comparison of the UPS He II ( $h\nu = 40.81$  eV) between the pentacene on Au(111) (left) and the pentacene on SnS<sub>2</sub> (right).

layer [ $\Phi(512 \text{ Å pentacene})$ ] giving

$$E_{\text{ion}}(512 \text{ Å pentacene}) = \text{HOMO}_{\text{cutoff}}(512 \text{ Å pentacene}) + \Phi(512 \text{ Å pentacene}) = 0.65 \text{ eV} + 4.76 \text{ eV} = 5.41 \text{ eV}$$

Sample charging is often an issue when measuring the orbital offsets of interfaces with organic materials, since the valence band and work function positions can no longer be precisely measured if the sample is charging. The procedure for determining the onset of charging is described in a previous work,<sup>12</sup> where the work function, as measured with both UPS and XPS, is plotted vs sample thickness. The pentacene films showed negligible sample charging even at thicknesses greater than 1000 Å, an indication of the high conductivity of pentacene thin films.<sup>25</sup> The above energy alignments were determined using the values at 512 Å pentacene thickness to ensure that there would be no influence of sample charging on the measured spectra.

#### IV. Energy Level Offsets

Our data do not allow the determination of whether the origins of the core level peak shift ( $\Delta C 1s$ ) in the pentacene layer are due to band bending or to differences in polarization energies. In the pentacene/Au(111) system, the gold substrate has a significantly larger polarization energy than the pentacene (4.9 vs 1.7 eV),<sup>22</sup> so the core hole remaining in the pentacene immediately adjacent to the gold surface should be screened more effectively than the core holes in bulk pentacene.

There is a stronger localized core level shift near the gold interface. This can be seen in the C 1s binding energy shift of approximately 0.3 eV in Figure 3 between 0 Å and around 16 Å thickness of the pentacene. This strong core level shift toward higher binding energies in the initial two or three molecular layers is similar to the shifts of the Xe 4f levels over the course

of a few monolayers of xenon on Pd(001).<sup>26</sup> After several molecular layer equivalents of pentacene, the binding energy decreases slightly by approximately 0.2 eV between 16 and 128 Å.

These early shifts can be attributed to the changing polarization environment of the core holes remaining after photoejection of the core electron. The initial C 1s binding energy of the first submonolayer (0.4 Å) of pentacene is 284.12 eV, which is comparatively low due to the final state screening induced by the strong polarization of the gold substrate. The C 1s binding energy reaches a maximum of 284.41 eV at about the 16–32 Å thickness, where the gold surface has already been completely covered by pentacene. At this point, the core hole screening is significantly reduced since the polarization energy of the adjacent pentacene molecules is significantly lower than that of the gold substrate. In addition, most of the C 1s signal still originates from surface molecules where the vacuum does not contribute to final state screening. Beyond several molecular layers (>32 Å), the remaining core holes in the pentacene are more thoroughly surrounded by adjacent pentacene molecules leading to a greater polarization-induced screening than in the very thin films (2–32 Å) of pentacene, yet still less than the polarization-induced screening caused directly by the gold.

It seems clear that the initial core level binding energy shifts can be attributed to differences in polarization environments between the interface and the bulk pentacene. Beyond these localized shifts near the interface, there is the overall net shift of 0.10 eV between the initial C 1s binding energy and the thick film (512 Å) of pentacene, the origins of which could be attributed to band bending or changes in the final state screening environments. This net shift extends well out into the bulk of the pentacene where the polarization environment becomes relatively constant. While part of this net shift could be contributions from changes in final state screening conditions,

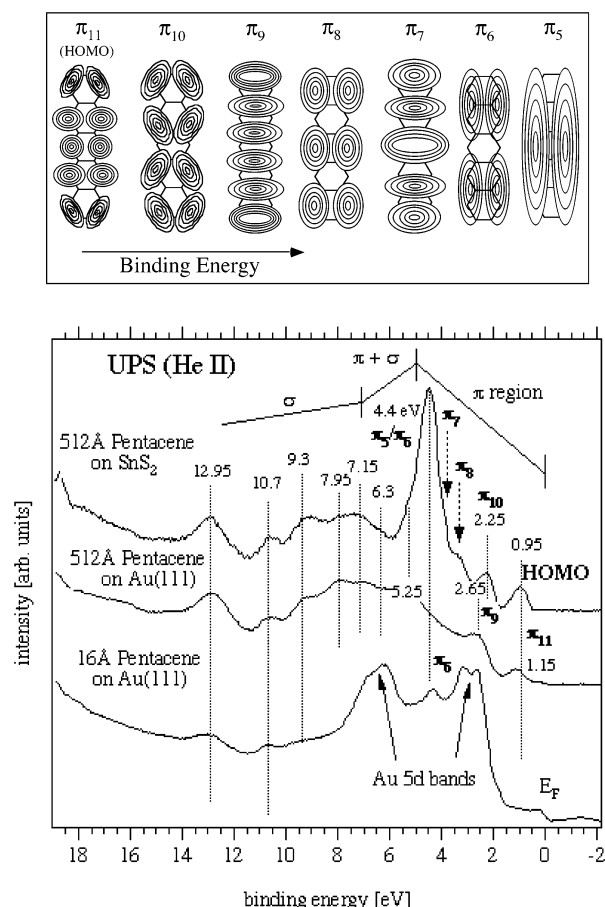


**Figure 9.** Comparison of the UPS He II of the 512 Å thick films of pentacene on the SnS<sub>2</sub> and Au(111) surfaces. The 16 Å film of pentacene on the Au(111) surface is also shown for comparison of the peak of the  $\pi_5/\pi_6$  band at  $\sim 4.4$  eV. Molecular orbital diagrams are based on diagrams in Ozaki, H. *J. Chem. Phys.* **2000**, *113*, 6361.

it is possible that at least part of this net shift could be attributed to band bending.

Core level shifts at the pentacene/SnS<sub>2</sub> interface may be more difficult to discern since the polarization energy of pentacene is likely close to that of SnS<sub>2</sub> (on the order of 3 eV). The shift of the Sn 3d emission peak for the vacuum-cleaved substrate to a higher binding energy as it becomes covered with pentacene indicates that band bending occurs in the SnS<sub>2</sub> substrate. This is expected because the SnS<sub>2</sub> crystal is a moderately doped inorganic semiconductor.

The C 1s shift between the very thin (0.4 Å) and the thick (512 Å) pentacene layers is a very small net shift ( $\Delta C\ 1s = 0.07$  eV), almost within the margin of error of the measurement process. This shift could be attributed to band bending in the pentacene film or to differences in polarization energies.

It should be noted that regardless of the origin of the core level shifts at the interfaces, they do resemble band bending-related shifts. As was stated by Ito and co-workers,<sup>27</sup> "the energy state of hole injection is similar to the hole state created by photoemission both effectively lowering the barrier for hole injection." A similar effect of lowering the electron injection barrier should occur if polarization effects are dominant; however, the exact magnitude of this effect remains unknown. It could be assumed that the magnitude of polarization effects for an electron would be similar to that for a hole, except that the direction of the band shift would be opposite of that for a hole. The band diagrams in Figure 5 reflect the core level shift modifications to the injection and interfacial dipole barriers. The

magnitude of the electron injection barriers ( $\Phi_{be}$  and  $\Delta LU-MO_{offset}$ ) is the maximum estimated barrier heights where band bending would be assumed. The lower values for the electron injection barriers are labeled in parentheses in Figure 5 to indicate a lower limit for the barrier height. The actual electron injection barrier heights are likely to be lower due to screening of the electron from the polarizable environment.

## V. Morphology of Pentacene Films

Comparing the He II spectra on each substrate (Figure 8) reveals a couple of notable spectral characteristics as the pentacene film gets thicker. The peaks are more clearly resolved in the HeII spectra than the HeI spectra because there is a reduced final state screening as a result of the higher energy incident photon.<sup>28</sup> The He II spectra for the 256 Å and greater thicknesses can be attributed almost entirely to the pentacene film. Despite the intense valence band photoemission peaks from the Au substrate (Figure 8, left), significant changes are discernible at low pentacene coverages. While the pentacene photoemission peaks are essentially at the same energy positions on both substrates, there are differences in their relative intensities.

The most obvious difference is the presence of the strong valence band peak at approximately 4.4 eV in the pentacene/SnS<sub>2</sub> system (Figure 8, right). This peak starts to emerge at approximately 1 Å average thickness and then continues to get stronger as the 1000 Å final film thickness is reached. This same peak appears as a small feature in the pentacene/Au(111) up to about 64 Å thick film, after which it is attenuated. Figure 9 shows UPS (He II) spectra for a 512 Å thickness of pentacene on SnS<sub>2</sub> and gold and the spectra of 16 Å of pentacene on gold. These show the presence of the 4.4 eV peak for the thinner layers of pentacene on gold and for thicker layers on SnS<sub>2</sub>. The peak at 4.4 eV in the He II spectra is in the purely  $\pi$  band region of the UP spectrum. The differences in the He II spectra are likely due to different orientations of the pentacene molecules within the film. The ionization energies of the thick pentacene films on the two substrates are different (5.07 eV on gold, 5.41 eV on the SnS<sub>2</sub>), perhaps due to the different orientations of the pentacene molecules.

Our measurements are not able to determine molecular orientation within the films with absolute certainty. However, several pieces of evidence indicate that the pentacene initially lies flat on both substrates. As the coverage increases, the molecules form crystallites on the Au(111) surface with the molecules oriented perpendicular to the substrate surface, on SnS<sub>2</sub> the molecules appear to either continue to lie flat or only gradually tilt upward forming 0.5–3  $\mu m$  polycrystalline domains as will be discussed below was previously seen by Ozaki.<sup>29</sup> Comparative analysis of the He II spectra coupled with scanning probe microscopy images may help elucidate the detailed growth behavior of the films.

Band assignments were made for some of the peaks in the He II spectra. These assignments were based on gas phase UPS of polyaromatic hydrocarbons as well as solid state UPS of pentacene films on stainless steel and HOPG, where transitions from 11 pentacene  $\pi$  molecular orbitals were assigned.<sup>30,29</sup> The peaks in the UPS in Figure 9 at 1.15 eV in the 512 Å thickness of pentacene on the Au(111) substrate correspond to the  $\pi_{11}$  molecular orbital, which is the HOMO of pentacene. The peak at approximately 4.4 eV corresponds to the  $\pi_5$  or  $\pi_6$  molecular orbitals of pentacene that are energetically very close together, according to the paper by Ozaki.<sup>29</sup> The  $\pi_5$  and  $\pi_6$  orbitals are strongly delocalized with only one node bisecting the molecule at the C2/C3 and C9/C10 bonds down the long axis of the

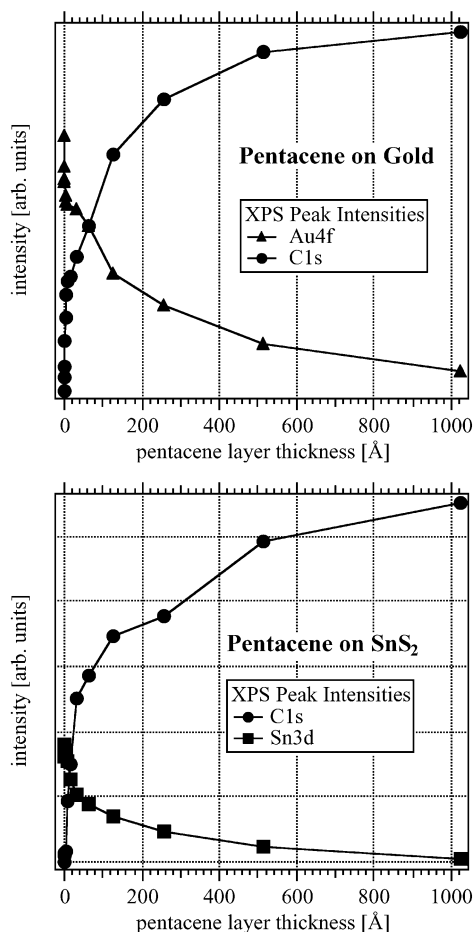


**Figure 10.** Cross-section-corrected intensities of the XPS core level peaks plotted as a function of the pentacene film thickness. Both the pentacene on Au(111) (top) and the pentacene on SnS<sub>2</sub> (bottom) revealed Stranski–Karastanov growth patterns.

molecule (see molecular structure of pentacene in Figure 1 for numbering system). The  $\pi_6$  band also has one node at the C6/C13 position of the pentacene molecule. The fact that one or both of these bands were predominant in the UPS on the SnS<sub>2</sub> substrate suggests that the molecules were oriented on the surface at an angle where the electron density cross-section normal to the sample surface was very high. In addition, this peak at 4.4 eV was initially present in the UPS for the first few molecular layers of pentacene on gold (up to about 50 Å) and then became attenuated at higher coverage of pentacene. This supports the notion that the pentacene molecules lay flat for several molecular layers before they start forming crystallites. The 4.4 eV peak is either very weak or absent in the UPS of thicker films on gold or stainless steel substrates where it was determined that the molecules were oriented nearly perpendicular to the surface. The presence of the strong  $\pi_5$  or  $\pi_6$  band peak for the pentacene on SnS<sub>2</sub> is likely attributed to a low molecular tilt angle of pentacene relative to the plane of the SnS<sub>2</sub> substrate.

The pentacene molecules are oriented flat on the gold surface for very thin films as determined from STM images detailed in other works.<sup>31,32</sup> Although STM imaging was attempted for thin pentacene films on the SnS<sub>2</sub> substrate, images could not be acquired, most likely due to a weak molecule–substrate interaction. Studies of pentacene films on HOPG using UPS and Penning ionization electron spectroscopy have revealed that pentacene molecules lie flat on HOPG at low coverages and then gradually tilt upward with increasing coverage.<sup>33</sup> Because

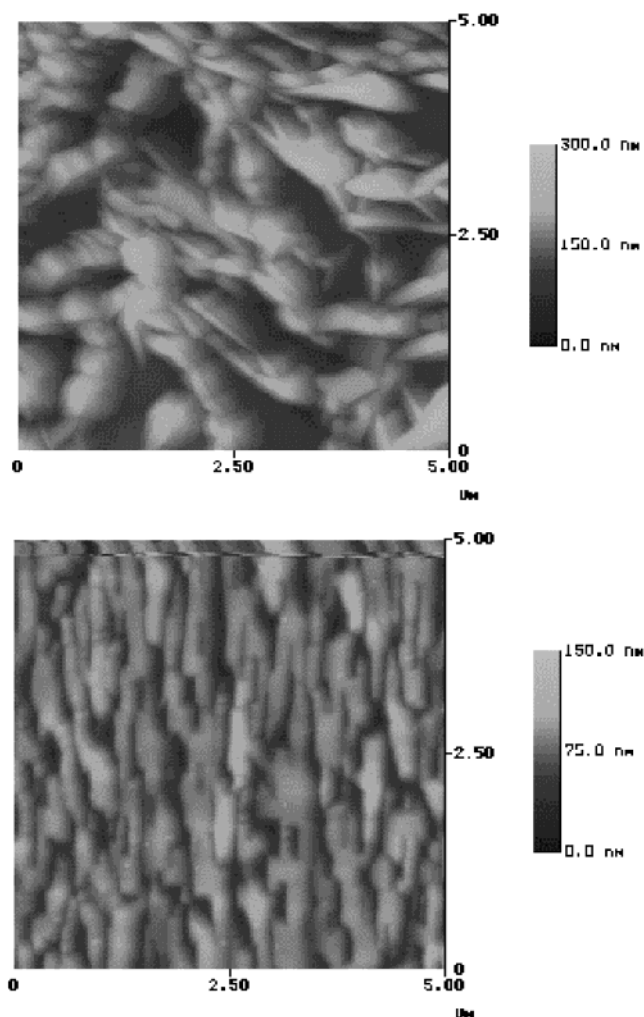


**Figure 11.** AFM images of 1000 Å pentacene films deposited on Au(111) (top) and SnS<sub>2</sub> (bottom).

HOPG has many similarities to SnS<sub>2</sub> such as low reactivity, a hexagonal close pack, and an atomically smooth surface, the initial adsorption of pentacene to each of these substrates is likely to be similar. As a result, we conclude that pentacene molecules initially lie flat on both the gold and the SnS<sub>2</sub> substrates.

For thicker films, it is known that polycyclic aromatic hydrocarbons, including pentacene, deposited at room temperature on rough metal surfaces, tend to form polycrystalline solids with the *ab* plane of each crystallite parallel to the substrate surface.<sup>10,29,34,35</sup> This orientation corresponds to the long axis (or *c*-axis) of the pentacene molecule oriented perpendicular to the substrate surface.<sup>36</sup> The UPS of thick films of pentacene on the gold surface (Figures 1 and 9) is very similar to that of pentacene films on stainless steel surfaces indicating similarities in morphology.<sup>29</sup>

An indication of the growth mode of the pentacene films deposited on the Au(111) substrate can be given by the cross-section corrected intensity of the C 1s and Au 4f peaks (Figure 10, top) plotted as a function of film thickness. The exponential decay of the Au 4f peak and the inverse exponential increase of the C 1s peak indicate that the pentacene film follows a Stranski–Karastanov growth pattern.<sup>37</sup> A similar trend is evident for the pentacene on SnS<sub>2</sub> (Figure 10, bottom) where the same type of growth mode is evident.

AFM images of 1000 Å thick films on both Au(111) and SnS<sub>2</sub> did reveal differences between the two films (Figure 11).



On the gold surface, the pentacene film (Figure 11, top) forms randomly spaced domains ranging in size from 500 nm to greater than 1  $\mu\text{m}$ . These sizes are significantly larger than the grain sizes of the Au surface (50–100 nm) indicating that the thick film growth is independent of the substrate morphology. The pentacene deposited on the SnS<sub>2</sub> substrate (Figure 11, bottom) yielded 3–5  $\mu\text{m}$  long and 100–300 nm wide domains of pentacene crystallites all oriented in the same general direction. These images were reproducible in different sample spots and with different scan angles. The pentacene films were rougher on the Au(111) surface (a Z-scale of 300 nm) whereas the pentacene on the SnS<sub>2</sub> surface was smoother (Z-scale was 150 nm). This supports our conclusion that the pentacene molecules are forming polycrystallites on the gold surface with the molecules oriented perpendicular to the substrate surface, whereas on the SnS<sub>2</sub> surface, the molecules seem to be forming smoother films with the molecular orientation likely more parallel to the substrate. The reasons for the unidirectional bulk orientation of the pentacene domains on SnS<sub>2</sub> is uncertain but likely attributed to the initial adsorption of pentacene on the substrate and the large areas of atomic flatness on cleaved SnS<sub>2</sub> crystals.

## VI. Summary

The energy level alignment for the pentacene/Au(111) and pentacene/SnS<sub>2</sub> interfaces was determined using a combined method of UPS and XPS. The hole and electron injection barriers for the pentacene/Au(111) interface were determined to be 0.55 and –1.30 eV, respectively, while a relatively large interface dipole barrier of 0.95 eV was observed. On the pentacene/SnS<sub>2</sub> interface, the hole and electron injection barriers were –1.89 and –1.44 eV, respectively, and there was a significantly smaller interface dipole magnitude of 0.26 eV. Polarization effects leading to changes in the final state screening environment contribute significantly to the core level energy shifts, particularly for systems such as the gold/pentacene where the polarization energies of the two materials are significantly different. Gradual core level shifts over a larger range of the pentacene film thicknesses provide evidence of possible band bending contributions as well.

Comparative analysis of the UP spectra revealed several distinct differences in the characteristics of the pentacene films on the two substrates and was attributed to the pentacene molecules being oriented perpendicular to the Au(111) and nearly parallel to the SnS<sub>2</sub> substrates. Detailed analysis of the UP spectra was done to explore the morphological differences of the pentacene on the two substrates and their relation to the interfacial energetics. AFM was used to investigate the thicker films revealing randomly oriented polycrystallites on the Au(111) surface and a lower surface roughness with oriented domains on the SnS<sub>2</sub>.

**Acknowledgment.** R. Schlaf is acknowledged for helpful discussions. The Department of Energy under contract DE-F603-96ER14625 has supported this work.

## References and Notes

- (1) Schön, J. H.; Berg, S.; Kloc, C.; Batlogg, B. *Science* **2000**, 287, 1022.

- (2) Lin, Y.-L.; Gundlach, D. J.; Nelson, S. F.; Jackson, T. N. *IEEE Trans. Electron Devices* **1997**, 44, 1325–1331.
- (3) Laquindanum, J. G.; Katz, H. E.; Lovinger, A. J.; Dodabalapur, A. *Chem. Mater.* **1996**, 8, 2542.
- (4) Schön, J. H.; Kloc, C.; Batlogg, B. *Appl. Phys. Lett.* **2000**, 77, 2473.
- (5) Schön, J. H.; Kloc, C.; Bucher, E.; Batlogg, B. *Nature* **2000**, 403, 408.
- (6) Schön, J. H.; Kloc, C.; Laudise, R. A.; Batlogg, B. *Phys. Rev. B* **1998**, 58, 12952.
- (7) Schön, J. H.; Kloc, C.; Batlogg, B. *Science* **2000**, 288, 2338.
- (8) Kasaya, M.; Tabata, H.; Kawai, T. *Surf. Sci.* **1998**, 400, 367–374.
- (9) Chen, X. L.; Lovinger, A. J.; Bao, Z.; Sapjeta, J. *Chem. Mater.* **2001**, 13, 1341.
- (10) Meyer zu Heringdorf, F.-J.; Reuter, M. C.; Tromp, R. M. *Nature* **2001**, 412, 517.
- (11) Schlaf, R.; Schroeder, P. G.; Nelson, M. W.; Parkinson, B. A.; Lee, P. A.; Nebesny, K. W.; Armstrong, N. R. *J. Appl. Phys.* **1999**, 86, 1499.
- (12) Schlaf, R.; Merritt, C. D.; Crisafulli, L. A.; Kafafi, Z. H. *J. Appl. Phys.* **1999**, 86, 5678.
- (13) Schlaf, R.; Parkinson, B. A.; Lee, P. A.; Nebesny, K. W.; Armstrong, N. R. *J. Phys. Chem. B* **1999**, 103, 2984.
- (14) Schlaf, R.; Schroeder, P. G.; Nelson, M. W.; Parkinson, B. A.; Merritt, C. D.; Crisafulli, L. A.; Murata, H.; Kafafi, Z. H. *Surf. Sci.* **2000**, 450, 142.
- (15) Schroeder, P. G.; Nelson, M. W.; Parkinson, B. A.; Schlaf, R. *Surf. Sci.* **2000**, 459, 349.
- (16) Ishii, H.; Sugiyama, K.; Yoachimura, D.; Ito, E.; Ouchi, Y.; Seki, K. *IEEE J. Sel. Top. Quantum Electron.* **1998**, 4, 24.
- (17) Ishii, H.; Oji, H.; Ito, E.; Hayashi, N.; Yoshimura, D.; Seki, K. *J. Lumin.* **2000**, 87–89, 61.
- (18) Hill, I. G.; Mäkinen, A. J.; Kafafi, Z. H. *Appl. Phys. Lett.* **2000**, 77, 1825.
- (19) Narioka, S.; Ishii, H.; Yoshimura, D.; Sei, M.; Ouchi, Y.; Seki, K.; Hasegawa, S.; Miyazaki, T.; Harima, Y.; Yamashita, K. *Appl. Phys. Lett.* **1995**, 67, 1899.
- (20) *CRC Handbook of Chemistry and Physics*, 73rd ed.; Lide, D. R., Ed.; CRC Press: Ann Arbor, 1992.
- (21) Pope, M.; Swenberg, C. E. *Electronic Processes in Organic Crystals and Polymers*; Oxford University Press: Oxford, 1999.
- (22) Sato, N.; Seki, K.; Inokuchi, H. *J. Chem. Soc., Faraday Trans. 2* **1981**, 77, 1621.
- (23) Schroeder, P. G.; France, C. B.; Parkinson, B. A.; Schlaf, R. *J. Appl. Phys.* **2002**, 91, 9095.
- (24) Schlaf, R.; Lang, O.; Pettenkofer, C.; Jaegermann, W. *J. Appl. Phys.* **1999**, 85, 2732.
- (25) Schön, J. H.; Kloc, C.; Batlogg, B. *Phys. Rev. B* **2001**, 63, 125304.
- (26) Kaindl, G.; Chiang, T.-C.; Eastman, D. E.; Himpsel, F. J. *Phys. Rev. Lett.* **1980**, 45, 1808.
- (27) Ito, E.; Oji, H.; Hayashi, N.; Ishii, H.; Ouchi, Y.; Seki, K. *Appl. Surf. Sci.* **2001**, 175/176, 407.
- (28) Ertl, G.; Küppers, J. *Low Energy Electrons and Surface Chemistry*, 2nd ed.; VCH Verlagsgesellschaft mbH: Weinheim, Germany, 1985.
- (29) Ozaki, H. *J. Chem. Phys.* **2000**, 113, 6361.
- (30) Boschi, R.; Clar, E.; Schmidt, W. *J. Chem. Phys.* **1974**, 60, 4406.
- (31) Schroeder, P. G.; France, C. B.; Park, J. B.; Parkinson, B. A. *J. Appl. Phys.* **2002**, 91, 3010.
- (32) (a) France, C. B.; Schroeder, P. G.; Parkinson, B. A. *Nano Lett.* **2002**, 2, 693. (b) France, C. B.; Schroeder, P. G.; Forsythe, J. C.; Parkinson, B. A. *Langmuir* **2003**, 19, 1274.
- (33) Harada, Y.; Ozaki, H.; Ohno, K. *Phys. Rev. Lett.* **1984**, 52, 2269.
- (34) Lee, K. O.; Gan, T. T. *Chem. Phys. Lett.* **1977**, 51, 120.
- (35) Kamura, Y.; Seki, K.; Inokuchi, H. *Chem. Phys. Lett.* **1975**, 30, 35.
- (36) Campbell, R. B.; Robertson, J. M.; Trotter, J. *Acta Crystallogr.* **1961**, 14, 705.
- (37) Argile, C.; Rhead, G. E. *Surf. Sci. Rep.* **1989**, 10, 277.